Chapter 2.

OFDM Wireless Communications

Contents

This chapter presents the most important aspects of OFDM wireless communications. It starts in **Section 2.1** with a general presentation of the time-variant multipath radio channels and the modeling of various effects. We discuss the WSSUS assumption and show how this is applied to baseband discrete channel modeling. We also show how the multipath components and their time-variant nature affect the channel properties, leading to frequency selectivity and Doppler spread. The channel estimation unit in the receiver must estimate these variations in time and frequency and compensate for them accordingly.

Section 2.2 introduces the principles of OFDM, including the signal model and its main parameters, such as the guard interval and the guard subcarriers. We then go on in **Section 2.3** to analyze the influence of channel Doppler variations on the received OFDM signal, for both slow-varying and fast-varying channels. In **Section 2.4** we discuss how other impairments affect the reception, such as timing and frequency errors, sampling clock frequency offset and additive noise.

2.1. Time-Variant Multipath Radio Channels

Mobile radio channels are essentially time-varying multipath channels. Multipath propagation occurs through scattering, reflection, and refraction, and strongly affects the quality of the reception. In order to compensate these impairments in the receiver, we need to understand their statistical properties and model them through an appropriate stochastic model.

2.1.1. The WSSUS Model

A very popular radio channel model is the "wide-sense stationary with uncorrelated scattering" (WSSUS) model introduced by Bello [1]. Assuming wide-sense stationarity, the channel is modeled as a linear superposition of uncorrelated echoes, as shown in (**2.1**). Each echo path p is characterized by a fixed delay τ_p and a time-varying gain $\gamma_p(t)$.

$$h(\tau, t) = \sum_{p=1}^{P} \gamma_p(t)\delta(\tau - \tau_p) \tag{2.1}$$

A stationary analog channel model is fully characterized by a two-dimensional scattering function. In time domain, it is the time-variant impulse response $h(\tau, t)$. We can also characterize the channel through the time-variant transfer function, Doppler-variant impulse response, or the Doppler-variant transfer function. All these two-dimensional functions, shown in **Figure 2.1** as Fourier pairs, carry the same information.

If the number of uncorrelated paths is assumed sufficiently large, the two quadrature components of the complex impulse response have a Gaussian distribution, according to the central limit theorem. The distribution of the phase and amplitude is uniform and Rayleigh respectively. It has been experimentally shown that a Gaussian model with zero mean fits many radio channels of practical interest: land mobile, HF ionospheric, indoor channels, and many others.

The wide-sense stationarity of the WSSUS model implies that the autocorrelation function $\varphi(\tau)$

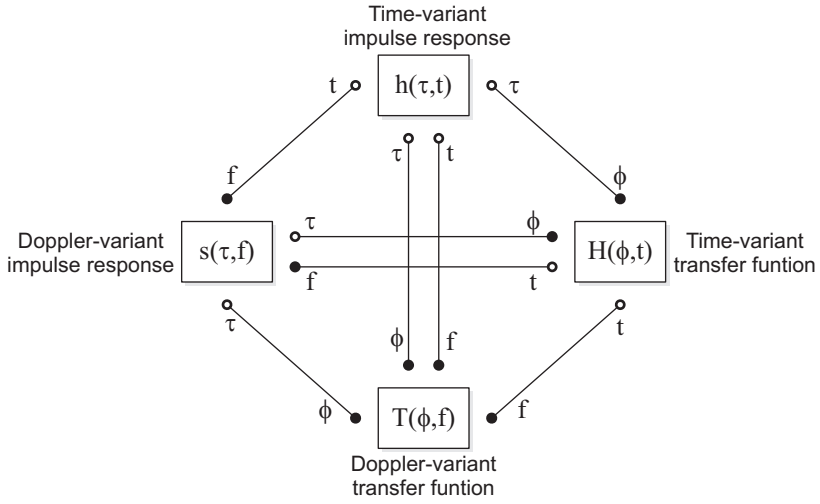

Figure 2.1.: Channel characterization functions

of the tap gains $\gamma(t)$ depends only on the difference between observation times τ.

$$\varphi(\tau) = E\{\gamma(t)\gamma^*(t-\tau)\} \tag{2.2}$$

The autocorrelation $\varphi(\tau)$ and the power spectral density $\Phi(f)$ of $\gamma(t)$ are Fourier pairs, according to the Wiener-Khinchin theorem:

$$\Phi(f) = \int_{-\infty}^{\infty} \varphi(\tau) e^{-j2\pi f\tau} d\tau \tag{2.3}$$

$\Phi(f)$ is also called Doppler spectrum and characterizes the fading rate of an echo path. The Doppler spectrum depends on the type of propagation.

2.1.2. Doppler Spectrum Types

Each received echo has a different Doppler shift corresponding to the cosine of the angle α between the velocity vector of the receiver and the ray's direction of arrival.

$$f_{Dsh} = \frac{v}{\lambda_c}\cos\alpha = \frac{v f_c}{c_0}\cos\alpha \tag{2.4}$$

where λ_c is the wavelength of the carrier frequency f_c and c_0 is the propagation speed in the free space. It can be seen that the Doppler shift increases linearly with the velocity and the carrier frequency.

For **land mobile channels**, a very large number of rays arrive at the receiver uniformly distributed in azimuth and with zero elevation. If the directivity of the receiver antenna is the same in all angles, the resulting normalized Doppler spectrum is given by the following formula:

$$\Phi_J(f) = \begin{cases} \frac{1}{\pi f_D} \frac{1}{\sqrt{1 - \left(\frac{f}{f_D}\right)^2}} & \text{if } |f| < f_D \\ 0 & \text{otherwise} \end{cases} \tag{2.5}$$

In this equation, f_D is the maximum Doppler shift, equal to vf_c/c_0. This Doppler spectrum is referred to as Jakes spectrum, although it has been introduced first by Clark [8] then popularized by Jakes [43]. The autocorrelation function is:

$$\varphi(\tau) = \mathcal{J}_0(2\pi f_D \tau) \tag{2.6}$$

where $\mathcal{J}_0(\cdot)$ is the zero-order Bessel function of the first kind.

Usually, the channel is modeled so that all taps have the same Doppler spread f_D regardless of delay.

For **indoor channels**, a very large number of rays arrive at the receiver uniformly distributed in elevation and azimuth. If the antenna is assumed to be either a short or a half-wave dipole, the resulting Doppler spectrum is flat in the $(-f_D, f_D)$ range, as shown by the following formula:

$$\Phi_U(f) = \begin{cases} \frac{1}{2f_D} & \text{if } |f| < f_D \\ 0 & \text{otherwise} \end{cases} \tag{2.7}$$

For **HF channels**, between 2 and 30 MHz, propagation occurs through ionospheric reflections. This band is used primarily for maritime, military, and aeronautical systems, as well as for long-distance broadcasting (AM). The multipath effect is caused by reflections of the radio signal on different layers of the ionosphere. In addition, multiple reflections can occur between ionosphere and the earth's surface.

Thus, the received signal is spread in time, containing several echoes or modes separated by a matter of milliseconds. The signal also experiences a frequency spread, as each mode fades due to the specifics of the ionospheric reflections.

The delay spread can range up to 6 ms, while the fading rate (Doppler spread) can be as high as 5 Hz [24]. More typical values are 2 ms and 1 Hz respectively. Northern trans-auroral paths can exhibit up to 10 ms of delay spread and 50 Hz of Doppler spread.

For HF channels, the WSSUS model has been experimentally validated by Watterson with on-air measurements [94]. The power spectrum of the taps has been determined to have a

Gaussian shape. Its normalized profile is given by:

$$\Phi_U(f) = \frac{1}{\sqrt{2\pi\sigma_D^2}} \exp\left(-\frac{(f - f_{Dsh})^2}{2\sigma_D^2}\right) \tag{2.8}$$

The Doppler spread D_{sp} is specified as the two-sided bandwidth that contains 68% of the power, i.e. $D_{sp} = 2\sigma_D$. Moreover, each path can exhibit an additional frequency shift f_{Dsh}, also denoted by D_{sh}. For a more in-depth treatment of the theory behind HF propagation with application to channel modeling, refer to the CCIR Report 549-2 [42] and Recommendation 520-1 [41].

2.1.3. Baseband Discrete Channel Modeling

The received continuous-time signal is down-converted to complex base-band and sampled with the sampling period T. We assume the A/D converter contains an ideal low-pass filter with bandwidth $1/T$. For the continuous-time channel in (**2.1**) at a certain time instant, the channel impulse response can be written:

$$h(\tau) = \sum_p \gamma_p \cdot \delta(\tau - \tau_p T) \tag{2.9}$$

where γ_p are the amplitudes of the incoming multipath components at that time instant, and τ_p are the path delays normalized to the sampling period T.

After sampling, the observed discrete channel impulse response becomes:

$$h_k = \sum_p \gamma_p \cdot \frac{\sin(\pi(k - \tau_p))}{\pi(k - \tau_p)} \tag{2.10}$$

where h_k is the response at lag k, i.e. for delay kT.

If τ_p is an integer, all the energy of path p is mapped to tap h_{τ_p}. In the general case when τ_p is not an integer, its energy will leak to all taps h_k. The actual leakage profile depends on the fractional part of τ_p, i.e. the inter-sample position of path p. **Figure 2.2** shows the contribution of a single path with $\gamma_p = 0.9$ to the discrete (sampled) impulse response, for three different inter-sample phases ϕ. As intuitively expected, the highest amount of leakage occurs for $\phi = 0.5$, when the path delay falls exactly in the middle between two sampling instants. The taps are complex and **Figure 2.2** shows their amplitudes only.

Equation (**2.10**) shows that a discrete channel can be modeled as a tapped delay line (FIR filter) with time-varying coefficients h_k, as shown in **Figure 2.3**. In general, the FIR filter is of infinite length even for finite-length echo delays and the tap gains are correlated even under the assumption of uncorrelated scattering [33]. In actual simulations, however, the length of

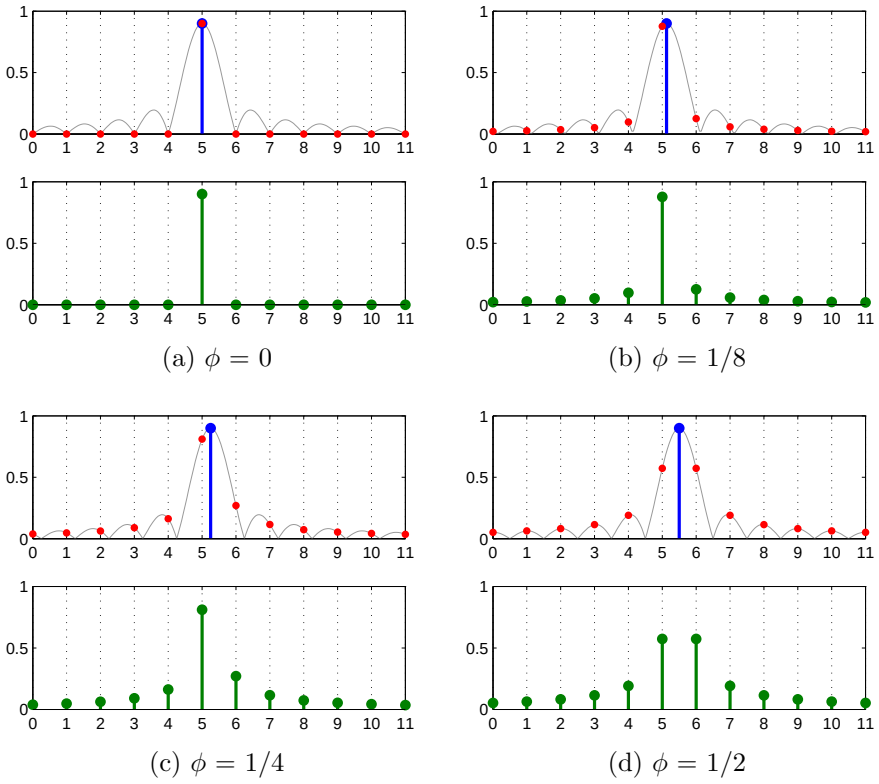

(a) $\phi = 0$ (b) $\phi = 1/8$

(c) $\phi = 1/4$ (d) $\phi = 1/2$

Figure 2.2.: Sampled channel impulse response for a single path

the channel impulse response can be considered finite. The length of the impulse response is denoted by L, so that the number of discrete taps including the first one h_0 is $L+1$. Moreover, the discrete taps can be assumed to be statistically independent in some simulation scenarios.

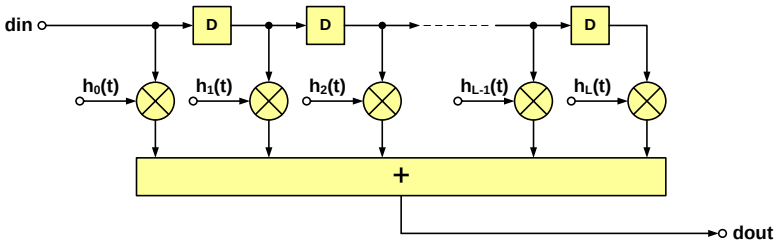

Figure 2.3.: Tapped delay line modeling of a WSSUS multipath channel

The time-varying taps h_k are discrete complex Gaussian processes, therefore their amplitude has a Rayleigh distribution and the phase is uniformly distributed in range $[0 \ldots 2\pi)$. The discretization affects the continuous time-variant impulse response $h(\tau, t)$ in the τ and t direction at the same time. The discrete time-variant CIR is now denoted by $h_k(n)$.

As mentioned in the previous section, the time-varying behavior of a discrete taps depend on its Doppler fading, which is characterized by three parameters: spectral profile type, spread,

and shift. The Doppler rate is usually much lower than the sampling rate. We define the normalized Doppler rate as the ratio between the actual Doppler rate and half the sampling rate (Nyquist limit) and we consider two examples to determine typical values thereof.

In the case of a DRM [21] receiver with a sampling frequency of 24 kHZ and a typical ionospheric HF channel with a Doppler spread of 2 HZ, the resulting discrete Doppler frequency is $2/12000 \approx 1.67 \cdot 10^{-4}$. For a DVB-T [20] receiver with a sampling frequency of 64/7 MHz, moving with 100 km/h, and receiving on a carrier frequency of 540 MHz, the maximum Doppler frequency is approx. $1.1 \cdot 10^{-5}$. In both cases, the discrete Doppler frequency is much smaller than the Nyquist limit 1.

2.1.4. Multipath Channel Delay Profiles

In order to provide different simulation scenarios and a consistent basis for performance comparison, various channel profiles have been proposed. For land mobile channels, power delay profiles have been proposed within the COST 207 working group [17], as well as by ITU for testing of various communication standards.

The COST 207 working group originally developed the proposed channel models in view of the emerging GSM mobile communication standard. Four families of channels were defined, corresponding to the four categories of propagation environments:

- Areas with rural character (*Rural Area*)
- Areas typical for cities and suburbs (*Typical Urban*)
- Urban areas with high building densities (*Bad Urban*)
- Hilly terrains (*Hilly Terrain*)

The COST 207 models are based on the WSSUS assumption. Another assumption is that the delay profile, or power density function, can be represented by one or more exponential decay functions. The delay power spectral density has the following expressions, for each of the four propagation environment. The delay τ is expressed in ns. **Figure 2.4** shows the four delay profiles graphically, for a delay τ of up to 20 μs.

Rural Area (AR):

$$P_d(\tau) = e^{-9.2\tau} \tag{2.11}$$

Typical Urban (TU):

$$P_d(\tau) = e^{-\tau} \tag{2.12}$$

Bad Urban (BU):

$$P_d(\tau) = \begin{cases} e^{-\tau} & 0 \leq \tau < 5\mu s \\ 0.5 \cdot e^{5-\tau} & 5\mu s \leq \tau \end{cases} \tag{2.13}$$

Hilly Terrain (HT):

$$P_d(\tau) = \begin{cases} e^{-3.5\tau} & 0 \leq \tau < 15\mu s \\ 0.1 \cdot e^{15-\tau} & 15\mu s \leq \tau \end{cases} \tag{2.14}$$

For convenience, **Figure 2.4** shows the logarithmic representation of these four delay profiles.

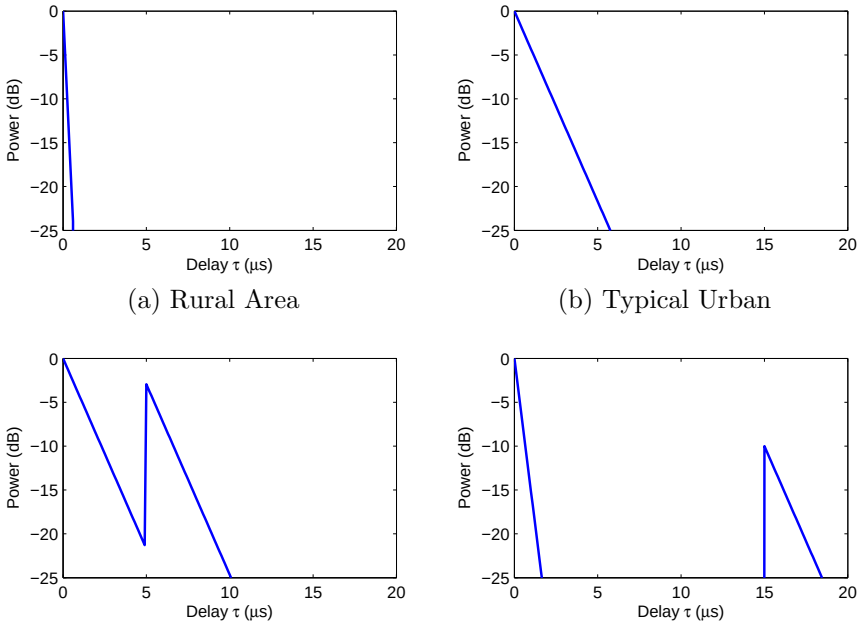

(a) Rural Area (b) Typical Urban

(c) Bad Urban (d) Hilly Terrain

Figure 2.4.: Delay profiles according to COST 207

COST 207 also provides discretized versions of the four power delay profiles. For each profile, two models with different complexities (number of taps) are proposed. All eight discretized models are listed in **Table 2.1**.

Discrete power delay profiles are also specified by ITU. Three profiles are proposed, each with two variants: 'indoor office', 'pedestrian', and 'vehicular'. The six discrete profiles are listed in **Table 2.2**.

For HF ionospheric propagation, the CCIR recommendation 520-1 [41] defines the well-known 'good', 'moderate', and 'poor' channel profiles. Each profile is defined by the number of taps, their delays, and the relative amplitudes, as well as by their Doppler spread D_{sp} and Doppler shift D_{sh}. **Table 2.3** shows the five multipath channels used in the specifications of the DRM standard [21].

Rural area (RA)		Typical urban (TU)		Bad urban (BU)		Hilly terrain (HT)	
4 taps	6 taps	6 taps	12 taps	6 taps	12 taps	6 taps	12 taps
Del ; Pow	Del ; Pow	Del ; Pow	Del ; Pow	Del ; Pow	Del ; Pow	Del ; Pow	Del ; Pow
0 ; 0	0 ; 0	0 ; -3	0 ; -4	0 ; -3	0 ; -7	0 ; 0	0 ; -10
0.2 ; -2	0.1 ; -4	0.2 ; 0	0.2 ; -3	0.4 ; 0	0.2 ; -3	0.2 ; -2	0.2 ; -8
0.4 ; -10	0.2 ; -8	0.6 ; -2	0.4 ; 0	1.0 ; -3	0.4 ; -1	0.4 ; -4	0.4 ; -6
0.6 ; -20	0.3 ; -12	1.6 ; -6	0.6 ; -2	1.6 ; -5	0.8 ; 0	0.6 ; -7	0.6 ; -4
;	0.4 ; -16	2.4 ; -8	0.8 ; -3	5.0 ; -2	1.6 ; -2	1.5 ; -6	0.8 ; 0
;	0.5 ; -20	5.0 ; -10	1.2 ; -5	6.6 ; -4	2.2 ; -6	17.2 ; -12	2.0 ; 0
;	;	;	1.4 ; -7	;	3.2 ; -7	;	2.4 ; -4
;	;	;	1.8 ; -5	;	5.0 ; -1	;	15.0 ; -8
;	;	;	2.4 ; -6	;	6.0 ; -2	;	15.2 ; -9
;	;	;	3.0 ; -9	;	7.2 ; -7	;	15.8 ; -10
;	;	;	3.2 ; -11	;	8.2 ; -10	;	17.2 ; -12
;	;	;	5.0 ; -10	;	10.0 ; -15	;	20.0 ; -14

Table 2.1.: COST 207 land mobile channel delay profiles (delay in us, power in dB)

Indoor office		Pedestrian		Vehicular	
A	B	A	B	A	B
Del ; Pow	Del ; Pow	Del ; Pow	Del ; Pow	Del ; Pow	Del ; Pow
0 ; 0	0 ; 0	0 ; 0	0 ; 0	0 ; 0	0 ; -2.5
0.05 ; -3.0	0.10 ; -3.6	0.11 ; -9.7	0.20 ; -0.9	0.31 ; -1	0.30 ; 0.0
0.11 ; -10.0	0.20 ; -7.2	0.19 ; -19.2	0.80 ; -4.9	0.71 ; -9	8.90 ; -12.8
0.17 ; -18.0	0.30 ; -10.8	0.41 ; -22.8	1.20 ; -8.0	1.09 ; -10	12.9 ; -10.0
0.29 ; -26.0	0.50 ; -18.0	;	2.30 ; -7.8	1.73 ; -15	17.1 ; -25.2
0.31 ; -32.0	0.70 ; -25.2	;	3.70 ; -23.9	2.51 ; -20	20.0 ; -16.0

Table 2.2.: ITU land mobile channel delay profiles (delay in us, power in dB)

Channel	Path	Delay τ_k	Gain (rms) ρ_k	Doppler shift D_{sh}	Doppler spread D_{sp}
#1	1	0	1	0	0.1 Hz
CCIR good	2	0.5 ms	1	0	0.1 Hz
#2	1	0	1	0.1 Hz	0.1 Hz
US consortium	2	0.7 ms	0.7	0.2 Hz	0.5 Hz
	3	1.5 ms	0.5	0.5 Hz	1.0 Hz
	4	2.2 ms	0.25	1.0 Hz	2.0 Hz
#3	1	0	1	0	1 Hz
CCIR poor	2	2 ms	1	0	1 Hz
#4	1	0	1	0	2 Hz
	2	4 ms	1	0	2 Hz
#5	1	0	0.5	0	0.1 Hz
	2	2 ms	1	1.2 Hz	2.4 Hz
	3	4 ms	0.25	2.4 Hz	4.8 Hz
	4	6 ms	0.0625	3.6 Hz	7.2 Hz

Table 2.3.: HF channel power delay profiles

Besides the above real-life channel delay profiles, it is desirable to introduce other delay profiles that help to evaluate the receiver performance with a finer granularity. Three of these profiles widely used in literature are: exponential decay profile, time-limited flat profile, and two multipath components with identical amplitudes.

The exponential decay profile has a single parameter, the real decay factor τ. The power of each channel tap h_k is computed as: $P_k = e^{\tau/k}$. The power decays very fast, therefore only a limited number of taps needs to be considered in simulation. In our simulations, we have set the threshold to -30 dB relative to the first tap. Only the taps whose power is above this threshold are considered. An example is shown in **Figure 2.5a** for $\tau = 3$.

The time-limited flat profile consists of L taps of constant power, as shown in **Figure 2.5b** for $L = 4$. The third profile consists of only two multipath components having the same power, with a delay difference of L sampling periods. **Figure 2.5c** shows this profile for $L = 4$

The discretized delay components define the discretized channel impulse response. The delay of the last multipath component is also referred to as the total delay spread of the channel. As the channel delay profile can have various shapes, the total delay spread alone does not carry much information about the channel delay profile. A better characterization thereof is provided by the RMS delay spread T_{RMS}, which is computed according to the formula:

$$T_{RMS} = T \cdot l_{RMS} = T \sqrt{\frac{1}{L+1} \sum_{l=0}^{L} P_l l^2} \tag{2.15}$$

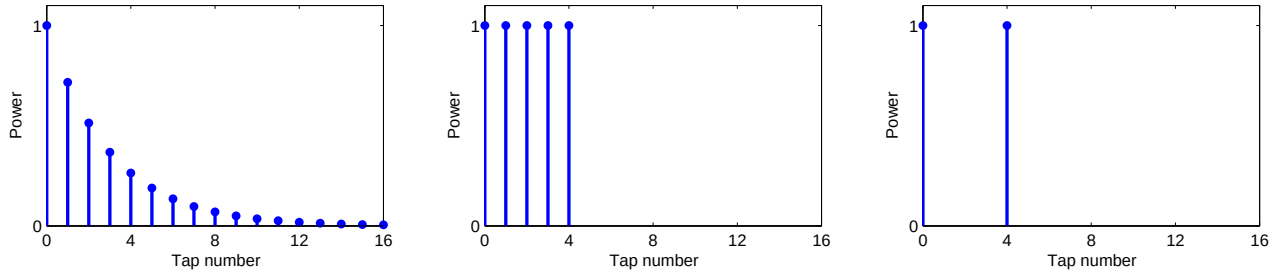

(a) Exponential decay (b) Time-limited flat (c) Two components

Figure 2.5.: Discrete channel delay profiles for simulation

where the channel taps are normalized, i.e. the channel has an unity power gain: $\sum_{l=0}^{L} P_l = 1$.

2.1.5. Frequency Selectivity

For the sampled base-band signal, the channel behaves like a discrete FIR filter, whose time spread introduces frequency selectivity. The longer the channel impulse response (CIR), the less smooth the channel transfer function (CTF). CIR and CTF are Fourier pairs and are both complex valued. Unlike a filter with real coefficients, the transfer function of a complex channel is not symmetrical. Since CIR is discrete with sampling period T, CTF is periodical with period $1/T$, the baseband ranging from $-1/2T$ to $1/2T$. In the following, the baseband is normalized to $-1 \ldots 1$, which makes the treatment of the problem independent of T.

Figure 2.6 shows the complex CIR and CTF for a realization of a Rayleigh channel having a negative exponential power-delay profile with $\tau = 3$. The channel has been normalized, so that it has an average unity gain, i.e. $\sum_{l=0}^{L} P_l = 1$. Besides the complex CTF, the figure also shows the power spectrum of the channel realization in dB, computed according to the following formula:

$$H_{dB}(f) = 10 \log_{10} |H(f)|^2 \tag{2.16}$$

where $H(f)$ is the complex CTF, i.e. Fourier transform of the CIR. We need to add at this point that the autocorrelation of the CTF is the power-delay profile of the channel in time domain. The inverse of the RMS delay of the latter is defined as the coherence bandwidth.

According to Parseval's theorem, the power gain of the channel can be computed from either its CIR or CTF according to the equation below. For a normalized channel, the average of the power gain G over many realizations is 1.

$$G = \sum_{l=0}^{L} h[l]^2 = \frac{1}{2\pi} \int_{-1}^{1} |H(f)|^2 df \tag{2.17}$$

It has been shown (**Figure 2.1**) that the Doppler effect leads to a time-variant channel impulse response $h(\tau, t)$. For an actual sampled system, $h(\tau, t)$ is discrete and limited along the τ axis.

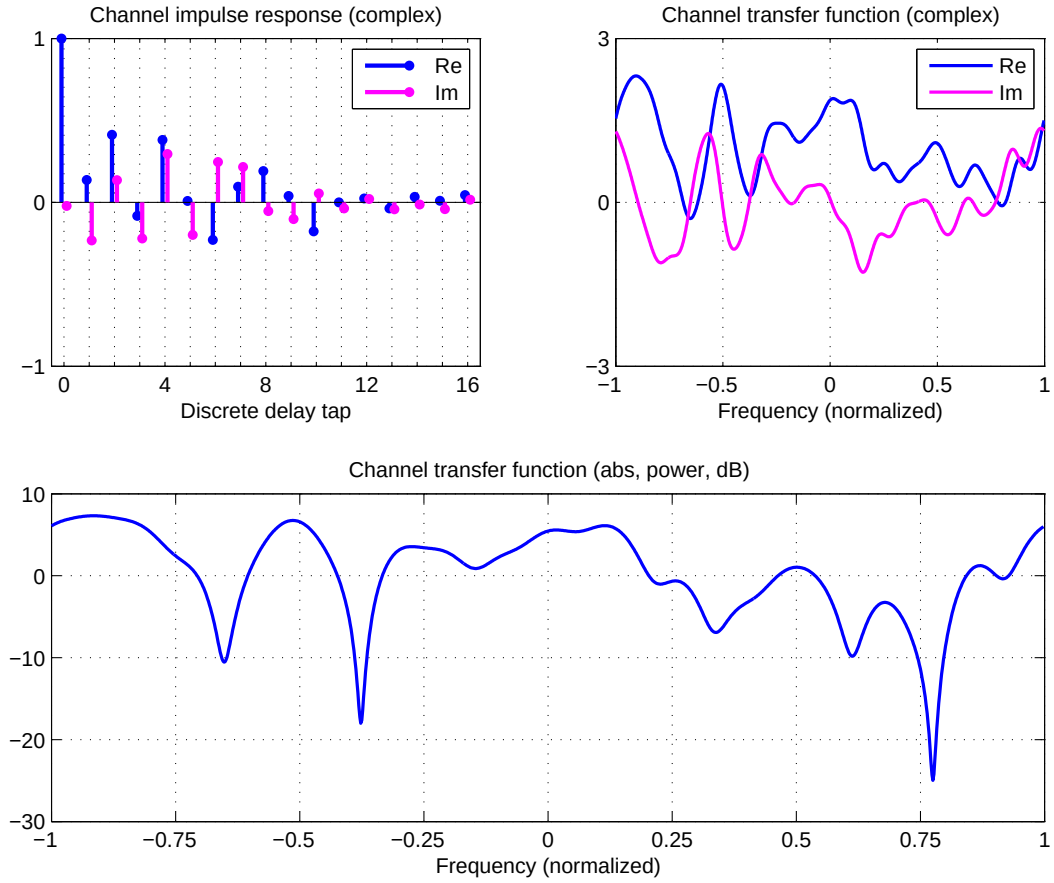

Figure 2.6.: CIR and CTF for an exponential channel realization

In this case, a more appropriate expression for CIR is $h_l(t)$ or $h(l,t)$. The time-variant nature of the CIR results in a time-variant CTF, which is also a function of two variables, $H(f,t)$.

As an example, we consider a DVB-T signal with a carrier frequency of 540 MHz and a receiver velocity of 100 km/h, which leads to a maximum Doppler spread of 50 Hz. The sampling rate is 64/7 MHz, which is typical for DVB-T baseband processing. An exponential decay power-delay profile of the multipath channel is assumed, with a decay constant τ of 3 taps. At the sampling rate of 64/7 MHz, this is about 0.33 μs, which is a very optimistic scenario. Even for the COST207 'Rural Area' profile, the impulse response is about three times longer ($tau = 0.92\mu s$).

The 3D representations of the time-variant CIR and CTF for this scenario are shown in **Figure 2.7** and **Figure 2.8** respectively, for a duration of 100 ms. **Figure 2.7** shows the absolute value of the complex CIR for the first 1+16 taps. **Figure 2.8** shows the complex CTF as power spectrum (in dB). It can be seen that various frequencies can briefly experience very deep fading.

Figure 2.9 shows the amplitude of the same complex CTF in **Figure 2.8** using an intensity

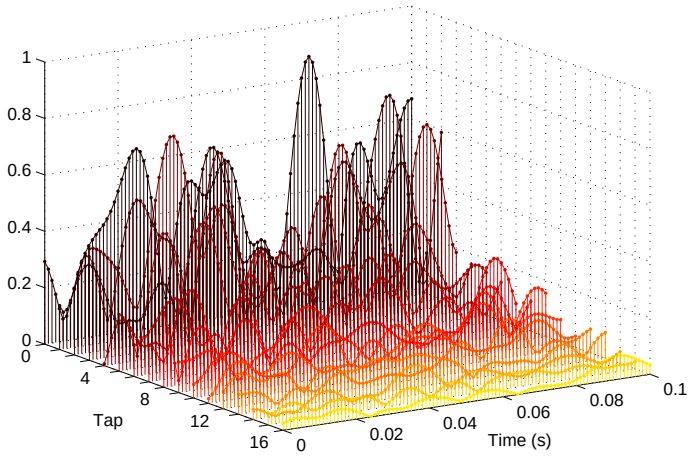

Figure 2.7.: Time-variant channel impulse response

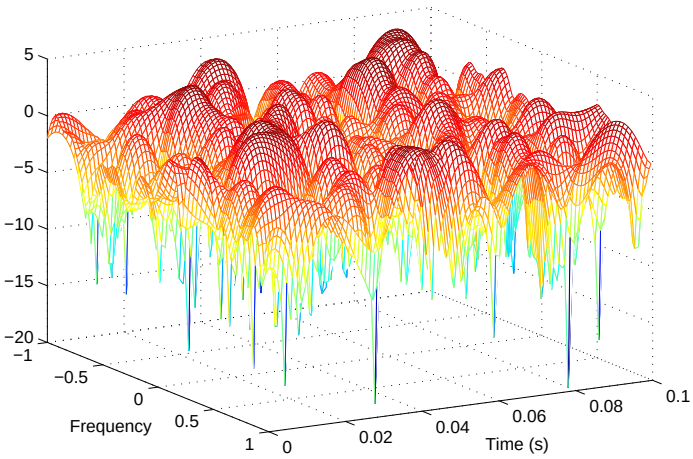

Figure 2.8.: Time-variant channel transfer function

map in 2D representation. Darker areas represent values close to zero. It must be mentioned here that the CTF is strictly limited in frequency by the sampling frequency, but unlimited in time. The example presented shows the CTF for a time window of 100 ms. It is now readily apparent that the purpose of the channel estimator is the estimation of the two-dimensional CTF. The actual process is presented in detail in **Chapter 5**.

For clarity, we also show in **Figure 2.10** the CTF in **Figure 2.8** at 6 time instances equally spaced between 0 and 100 ms

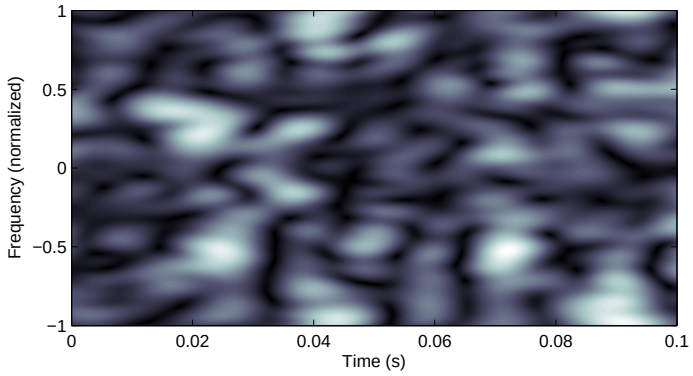

Figure 2.9.: Time-variant channel transfer function (2D)

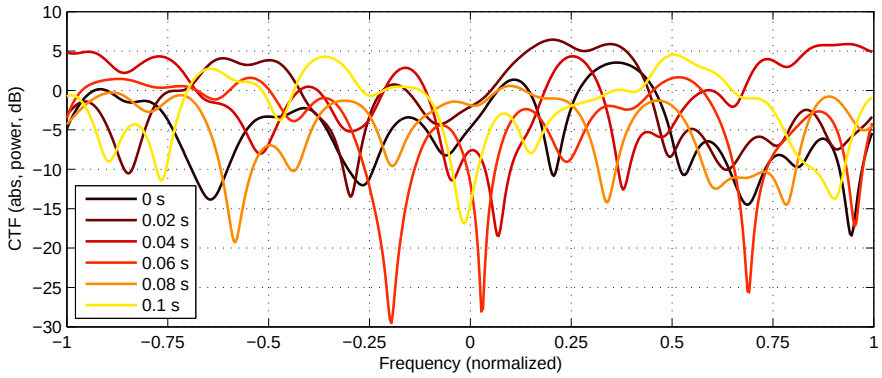

Figure 2.10.: CTF at various instants

2.2. Principles of Orthogonal Frequency-Division Multiplexing

Orthogonal frequency-division multiplexing (OFDM) [3] is a high-efficiency modulation scheme in which the channel is divided into many narrower subchannels. In doing so, the symbol length is increased significantly, which helps to avoid inter-symbol interferences (ISI) due to multipath reflections. The subcarriers experience flat fading since the subchannel bandwidth is chosen to be significantly lower than the coherence bandwidth of the channel. This ensures a robust behavior in frequency-selective channels.

The essential advantages of the OFDM modulation are a high spectral efficiency, robustness against multipath effects (ISI, frequency selectivity), and simplified channel equalization. Unlike single-carrier systems, there is no need for complex adaptive equalizers in time domain. The only notable disadvantage is the relative sensitivity to carrier frequency offset and Doppler spread, which cause inter-carrier interferences (ICI).

The basic principle of OFDM, shown in **Figure 2.11**, is that the samples to be transmitted are divided into N parallel streams, updated with a symbol period T_S. The symbol index is

denoted by s. Each stream modulates a separate subcarrier of frequency f_k, where k is the subcarrier index $\in [0; N-1]$. The subcarrier frequencies obey the relationship $f_k = k \cdot f_0$, where $f_0 = 1/T_S$. This relationship (equal spacing) ensures their orthogonality, which enables their perfect separation in the receiver, provided that no frequency shift occurs.

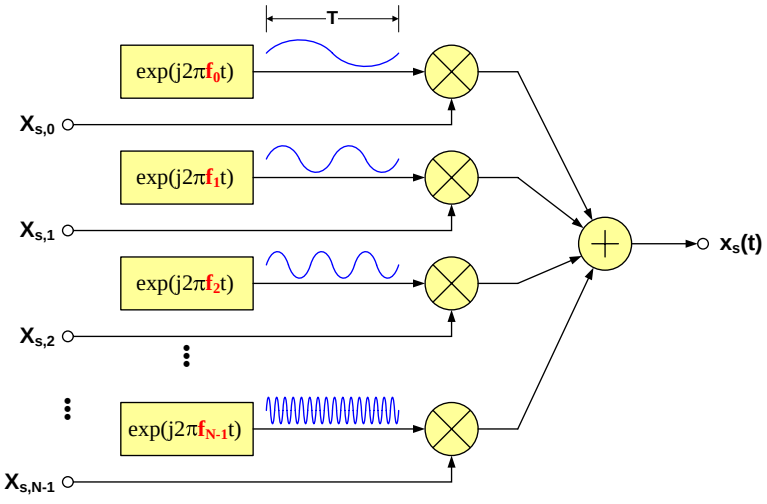

Figure 2.11.: OFDM modulation

2.2.1. Signal Model

The baseband signal is generated by weighting the complex unmodulated subcarriers $\exp(j2\pi f_k t)$ with the complex information-bearing samples $X_{s,k}$. For each symbol s, the resulting signal $x_s(t)$ is

$$x_s(t) = \sum_{k=0}^{N-1} X_{s,k} e^{j2\pi(k/T_S)t} \qquad 0 \le t \le T_S \tag{2.18}$$

The continuous-time OFDM signal $x_{tx}(t)$ is obtained by concatenating successive symbols $x_s(t)$:

$$x_{tx}(t) = \sum_{s=-\infty}^{\infty} x_s(t) u(t - sT_S) = \sum_{s=-\infty}^{\infty} \sum_{k=0}^{N-1} X_{s,k} e^{j2\pi(k/T_S)(t-sT_S)} u(t - sT_S) \tag{2.19}$$

where $X_{s,k}$ is the complex data symbol transmitted on subcarrier k in the interval $[sT_S, (s+1)T_S]$ and $u(t)$ is the symbol mask defined as:

$$u(t) = \begin{cases} 1, & 0 \le t < T_S \\ 0, & \text{otherwise} \end{cases} \tag{2.20}$$

So far, it has been assumed that the processing is performed in the continuous-time analog domain, which is convenient for illustrating the principles of OFDM. In practical systems,

however, the entire baseband processing is performed in the discrete-time digital domain. The sampling frequency f is exactly T_S/N, so that the number of sampling periods per symbol is N. Knowing that $f_k = k/T_S$ and expressing $X_{s,k}$ as $X_s(k)$, (**2.18**) can be rewritten as:

$$x_s(n) = \sum_{k=0}^{N-1} X_s(k) e^{j2\pi kn/N} \qquad n = 0, 1, \ldots, N-1 \tag{2.21}$$

The above equation shows that the discrete OFDM modulation is equivalent to an N-point inverse discrete Fourier transform (IDFT). This greatly simplifies the hardware realization, since the IDFT can be very efficiently implemented using the FFT algorithm when N is a power-of-two. The number of complex multiplications per symbol is thus reduced from N^2 to $N \log_2 N$, which is especially important for large symbol sizes.

Using matrix notation and dropping the s index, (**2.21**) can be written as:

$$\mathbf{x} = \mathbf{F}^{-1}\mathbf{X} \tag{2.22}$$

where $\mathbf{x}$ and $\mathbf{X}$ are N-element vertical vectors of the values $x_s(n)$ and $X_s(k)$ respectively, and $\mathbf{F}$ is the N × N Fourier matrix with elements $\exp(j2\pi kn/N)$, where $k, n \in [0, N-1]$.

2.2.2. Guard Interval and Guard Subcarriers

Although the symbol period T_S has been extended to N times the sampling rate, the OFDM modulation by itself is still not immune to ISI, which occur because of the channel delay spread. The solution consists in inserting a guard interval between the symbols, which eliminates ISI completely if its length exceed the channel delay spread. The most popular solution is to insert a copy of the last part of the OFDM symbol, as shown in **Figure 2.12**, referred to as cyclic prefix (CP).

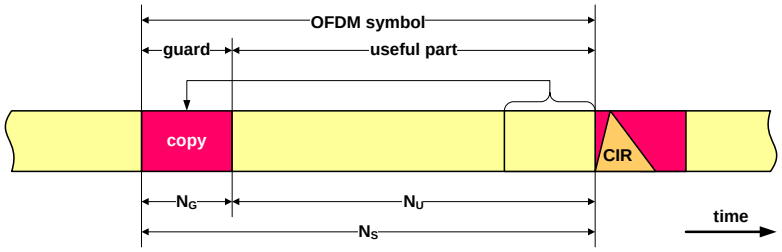

Figure 2.12.: Cyclic prefix (guard interval) insertion

The guard interval results in a lower spectral efficiency because of the decreased symbol rate. Therefore, its relative length must be kept low, e.g. 1/4. Another drawback is that additional sender power is needed for the cyclic prefix. Moreover, this leads to a slight SNR loss in the receiver.

The two main design parameters of an OFDM system are the channel bandwidth and the worst-case channel delay spread. The channel bandwidth determines the sampling rate, while the channel delay spread imposes the lower limit for the cyclic prefix. The raw data rate depends directly on the sampling frequency and the relative length of the guard interval. The absolute length of the latter is chosen to be slightly longer than the worst-case delay spread in the environment for which the system is designed. The useful symbol size is then chosen so as to ensure an acceptable efficiency, e.g. at least 4 time longer. The longer the symbol, the higher the efficiency, but at the cost of increased receiver complexity and decreased robustness against Doppler effects. Ultimately, the useful symbol size is directly proportional to the channel delay spread and the desired data rate.

The duration of the useful symbol is denoted by T_U, and the duration of the guard interval by T_G. Thus, the total duration of a full symbol is $T_S = T_U + T_G$. The corresponding number of samples are N_U (or N), N_G, and N_S. N_U and N_G are usually powers-of-two, as this simplifies the implementation. One notable exception is Digital Radio Mondiale [21], where the symbol length is a power-of-two only in one out of the four modes specified.

Modifying (**2.19**), the OFDM baseband signal in the continuous-time domain can be now expressed as:

$$x_{tx}(t) = \sum_{s=-\infty}^{\infty} \sum_{k=0}^{N-1} X_{s,k} e^{j2\pi(k/T_U)(t-T_G-sT_S)} u(t - sT_S) \tag{2.23}$$

In an OFDM system, the number of subcarriers N is equal with the number of samples in the useful part of the symbol. The spectrum of the complex OFDM signal ranges from $-f/2$ to $f/2$, where f is the sampling frequency. The N subcarriers have the same spacing $\Delta f = 1/T_S = f/N$. Subcarrier spacing is an important property that determines the robustness of the system against frequency offsets and Doppler variations. For a given sampling rate, the carrier spacing decreases for large N, leading to an increased sensitivity to frequency errors.

In practical systems, in order to simplify the channel filtering and the rejection of adjacent channels, a number of guard subcarriers at the margins of the spectrum are not transmitted. The DC subcarrier is also suppressed, as the transmission of a DC level would worsen the signal dynamic range. The indices of the active subcarriers at the margins of the spectrum are denoted by k_{min} and k_{max} respectively. As an example, **Figure 2.13** shows the active carriers for the IEEE 802.11a wireless LAN standard [38], which has a symbol size of 64.

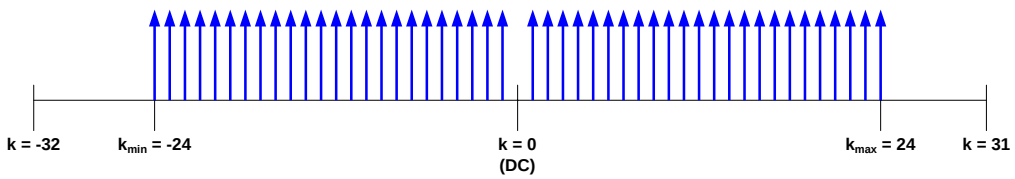

Figure 2.13.: Guard subcarriers and DC suppression

Throughout this work, the DC-centered subcarrier range $-N/2 \ldots N/2-1$ will be used instead

of the $0 \ldots N-1$ native DFT range. The mapping simply consists in rotating the index vector with $N/2$.

In order to keep the analysis independent of actual durations and frequencies, e.g. sampling rate, symbol duration, or Doppler frequency, only normalized quantities are considered throughout this work. Durations are expressed in sampling periods $t_s = 1/f_s$, whereas frequencies are normalized to the sampling frequency f_s.

2.3. The Influence of Channel Doppler Variations

The received continuous-time OFDM signal $y_{rx}(t)$ is the convolution of the transmitted signal $x_{tx}(t)$ in (**2.23**) with the time-variant channel impulse response $h_i(t)$:

$$y_{rx}(t) = h_i(t) * x_{tx}(t) = \sum_i h_i(t) \sum_s \sum_k X_{s,k} e^{j2\pi(k/T_U)(t-T_G-sT_S-\tau_i)} u(t - sT_S - \tau_i) \qquad (2.24)$$

In order to analyze the influence of the channel we consider an OFDM system that consists of a modulator, a multipath channel, and a demodulator, assuming that the frequency and timing synchronization in the receiver are perfect. The baseband model is shown in **Figure 2.14**.

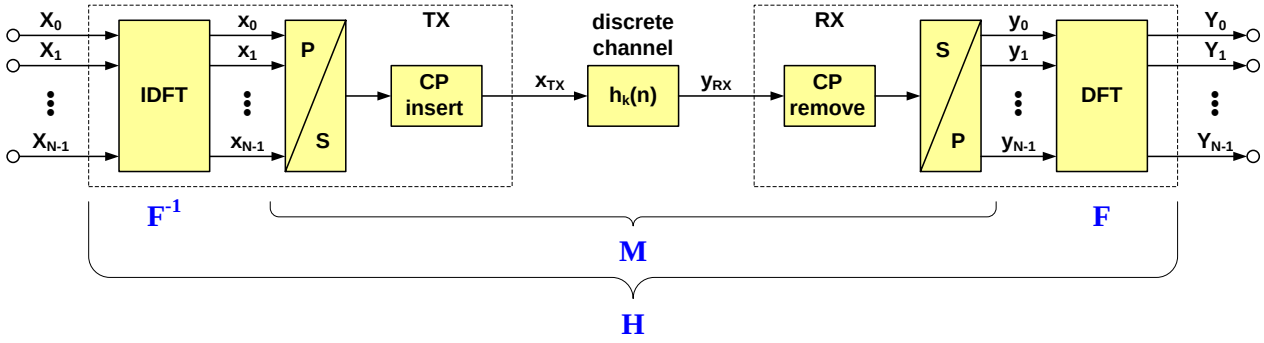

Figure 2.14.: OFDM system model for transmitter and receiver

The complex baseband-equivalent channel model is discrete and besides the actual time-variant multipath wireless channel, it also includes various hardware elements in the transmitter and receiver, as shown in **Figure 2.15**. For this analysis, the channel is first assumed to be noiseless.

The cyclic prefix transforms the convolution of the transmitted signal with the time-variant channel impulse response into a circular convolution, according to the equation below.

$$y_n = h_k(n) \circledast x_n \qquad (2.25)$$

where $h_k(n)$ is the time-variant complex channel transfer function, in which k is the discrete tap index and n is the sample index of the time-variant complex taps.

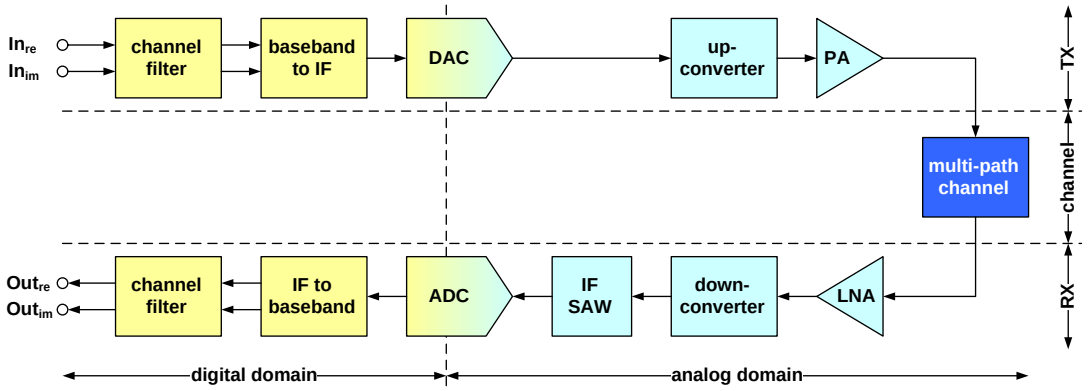

Figure 2.15.: Discrete baseband channel model

Using matrix notations, the same equation can be expressed as:

$$\mathbf{y} = \mathbf{M} \cdot \mathbf{x} \tag{2.26}$$

where $\mathbf{x} = [x_0, x_1, \ldots, x_{N-1}]^T$ and $\mathbf{y} = [y_0, y_1, \ldots, y_{N-1}]^T$. The matrix M is referred to as circular channel matrix and has the following expression:

$$\mathbf{M} = \begin{bmatrix} h_0(0) & 0 & \cdots & 0 & h_G(0) & \cdots & h_2(0) & h_1(0) \\ h_1(1) & h_0(1) & 0 & \ddots & 0 & h_G(1) & \ddots & h_2(1) \\ \vdots & h_1(2) & h_0(2) & 0 & \ddots & \ddots & \ddots & \vdots \\ \vdots & \ddots & \ddots & \ddots & \ddots & \ddots & 0 & h_G(G-1) \\ h_G(G) & \cdots & \cdots & h_1(G) & h_0(G) & 0 & \cdots & 0 \\ 0 & \ddots & \ddots & \ddots & \ddots & \ddots & \ddots & \vdots \\ \vdots & \ddots & \ddots & \ddots & \ddots & \ddots & h_0(N-2) & 0 \\ 0 & \cdots & 0 & h_G(N-1) & \cdots & \cdots & h_1(N-1) & h_0(N-1) \end{bmatrix} \tag{2.27}$$

where the shorthand notation $N_G = G$ has been used.

2.3.1. Slow-Varying Channels

If the Doppler variation of the channel is slow enough, so that the channel impulse response can be considered constant for the duration of one symbol ($h_k(n) \approx h_k(n+N)$), the circular

channel matrix $\mathbf{M}$ has constant diagonals.

$$\mathbf{M} = \begin{bmatrix} h_0 & 0 & \cdots & 0 & h_G & \cdots & h_2 & h_1 \\ h_1 & h_0 & 0 & \ddots & 0 & h_G & \ddots & h_2 \\ \vdots & h_1 & h_0 & 0 & \ddots & \ddots & \ddots & \vdots \\ \vdots & \ddots & \ddots & \ddots & \ddots & \ddots & 0 & h_G \\ h_G & \cdots & \cdots & h_1 & h_0 & 0 & \cdots & 0 \\ 0 & \ddots & \ddots & \ddots & \ddots & \ddots & \ddots & \vdots \\ \vdots & \ddots & \ddots & \ddots & \ddots & \ddots & h_0 & 0 \\ 0 & \cdots & 0 & h_G & \cdots & \cdots & h_1 & h_0 \end{bmatrix} \tag{2.28}$$

A circular matrix is diagonalizable, i.e. it can be written in the form:

$$\mathbf{M} = \mathbf{PDP^{-1}} \tag{2.29}$$

where $\mathbf{D}$ is a diagonal N×N matrix whose entries are the eigenvalues of $\mathbf{M}$, and $\mathbf{P}$ is an invertible N×N matrix whose columns are eigenvectors corresponding to the eigenvalues in $\mathbf{D}$. The necessary and sufficient condition for an N×N matrix to be diagonalizable is that it has N linearly independent eigenvectors.

The N eigenvectors $\mathbf{v_k}$ of matrix $\mathbf{M}$ in (**2.28**) are the normalized column vectors of the DFT matrix:

$$\mathbf{v_k} = \frac{1}{\sqrt{N}} \left[1, e^{-j\frac{2\pi}{N}1k}, e^{-j\frac{2\pi}{N}2k}, \ldots, e^{-j\frac{2\pi}{N}(N-1)k}\right]^T \quad k = 0, \ldots, N-1 \tag{2.30}$$

The eigenvalues D_k in diagonal matrix $\mathbf{D}$, corresponding to the eigenvectors $\mathbf{v_k}$, have the following expression:

$$D_k = \sum_{n=0}^{N-1} h_n \cdot e^{-j\frac{2\pi}{N}kn} \quad k = 0, \ldots, N-1 \tag{2.31}$$

It can be seen that the eigenvalues D_k are actually the DFT of the channel impulse response h_n. This means that the diagonal matrix $\mathbf{D}$ is actually the transfer matrix $\mathbf{H}$ of the OFDM system in **Figure 2.14**.

$$\mathbf{H} = \mathbf{F^{-1}MF} \tag{2.32}$$

The conclusion is that for slow-varying channels, the OFDM transfer matrix is diagonal. Therefore, no ICI occur and each subcarrier is affected only by a multiplicative constant, i.e. the elements on the main diagonal. The transfer function can be simply written as:

$$Y_k = X_k \cdot H_k \tag{2.33}$$

This allows for simple channel estimation and equalization, which is one of the main advantages of OFDM. The equalization consists only in dividing the received data Y_k by the channel transfer function estimates $\tilde{H}_k$, as shown in **Figure 2.16**. Channel estimation remains the only challenging task.

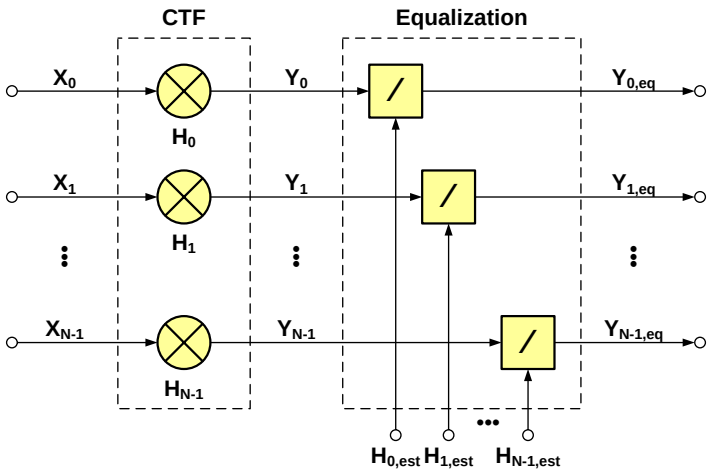

Figure 2.16.: Channel equalization in OFDM

2.3.2. Fast-Varying Channels

If the CIR varies significantly during a symbol, the diagonals of the circular channel matrix $\mathbf{M}$ cannot be considered constant anymore and its eigenvectors are no longer the columns of the DFT matrix. Therefore, the frequency-domain channel transfer matrix $\mathbf{H} = \mathbf{F}^{-1}\mathbf{M}\mathbf{F}$ is no longer diagonal, which leads to inter-carrier interferences (ICI). The amount of ICI depends on how much the channel changes during the useful part of a symbol, i.e. on the product $f_D \cdot T_u$.

The channel estimation involves now the estimation of all the elements of matrix $\mathbf{H}$, not only of its main diagonal. A mathematical apparatus for estimating this matrix is presented in [84], but no implementation is suggested, as the complexity of the estimator would be prohibitive. The equalization would be extremely complex as well, involving the division of a vector by a matrix. This is a very important topic, as the ICI due to Doppler variations are the main performance limiting factor at higher receiver velocities, as it can be observed in **Figure 5.7**.

According to [9] the normalized power of the ICI caused by a single fading multipath component with average amplitude h_i and a Jakes Doppler spectrum with frequency f_D is given by:

$$\sigma^2_{ICI,i} \approx \frac{\pi^2}{6}|h_i|^2(f_D T_U)^2 \tag{2.34}$$

As the channel taps can be considered uncorrelated, the total fading ICI power can be obtained by summing the contributions of all taps. Considering a normalized channel, with unity average

power gain $\sum_i |h_i|^2$, the total Doppler fading ICI power becomes:

$$\sigma^2_{ICI} \approx \frac{\pi^2}{6}(f_{Dn}N_U)^2 \tag{2.35}$$

where f_{Dn} is the normalized discrete Doppler rate.

The highest Doppler frequency that the system can handle is limited by the pilot spacing D_s in time domain, according to the sampling theorem: $f_{Dmax} = (2D_sN_s)^{-1}$. The worst-case fading ICI power, which corresponds to this frequency, is given by the equation:

$$\sigma^2_{ICI,max} \approx \frac{\pi^2}{24}\left[\frac{1}{D_s(1+N_G/N_U)}\right]^2 \approx \frac{\pi^2}{24D_s^2} \tag{2.36}$$

As an example we consider a DVB-T system with a symbol size of 2048 (2k mode) and a relative cyclic prefix length of 1/32. Since the pilot spacing in time is $D_s = 4$, the maximum Doppler frequency that the system can handle is approx. 2^{-14}. From (**2.36**), the worst-case ICI noise power is in this case $\sigma^2_{ICI,max} \approx 0.008$, which is also confirmed experimentally.

Figure 2.17 shows the experimental channel transfer function and a few ICI contributions for the above DVB-T system, considering a multipath channel with an exponential-decay profile and a decay constant $\tau = 8$. The ICI from four neighboring subcarrier pairs are considered. As expected, the nearest 2 subcarriers produce the highest ICI, which is already some 20 dB below the CTF, close to the theoretical 0.008 figure resulting from (**2.36**).

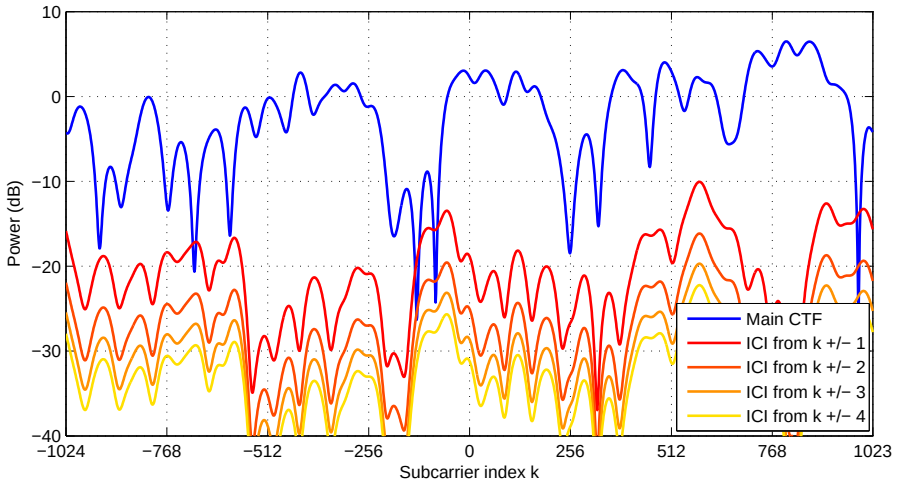

Figure 2.17.: ICI caused by fast Doppler variations

The conclusion is that the errors introduced by the fading ICI have typically low levels and can be treated as additive noise.

2.4. The Influence of Various Channel Impairments

2.4.1. Timing Synchronization Errors

Assuming a quasi-static or slowly-varying multipath channel, we consider now that the the timing synchronization is not perfect and introduce residual errors. Timing errors occur when the cyclic prefix is not correctly detected, which causes the useful N_U symbol samples to be extracted either too early (negative timing error) or too late (positive error). Positive timing errors result immediately in ISI with the next symbol, whereas negative errors lead only to an incremental phase shift of the samples in frequency domain because of the cyclic prefix. Therefore, if the timing synchronizer (guard interval removal) errs, it should err toward negative errors. Nevertheless, if the negative error exceeds he difference between the length of the guard interval and the length of the CIR, ISI with the previous symbol will occur.

The CIR length is denoted with L and must not exceed the guard interval length N_G to avoid ISI. **Figure 2.18** shows different scenarios when extracting the useful samples of the symbol.

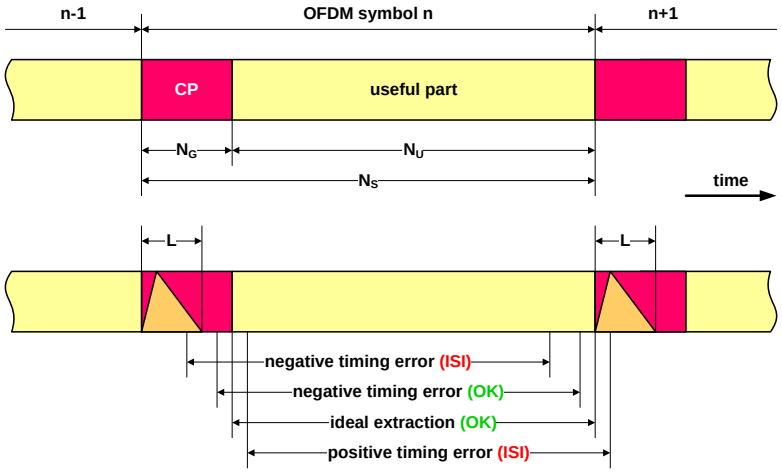

Figure 2.18.: Timing errors in useful symbol extraction

Provided that $N_G > L$, the allowed range for the timing offset error n_ε is:

$$L - N_G \leq n_\varepsilon \leq 0 \tag{2.37}$$

As long as n_ε is in the allowed range no ISI occur. The timing error n_ε is equivalent with delaying the CIR, which results in an incremental rotation of the CTF samples since CIR and CTF are Fourier pairs. For each increment of n_ε, an additional incremental rotation of $2\pi/N$ per subcarrier take place, or an overall rotation of 2π from subcarrier 0 to subcarrier N-1. Mathematically, the rotation of the channel transfer function $H(k)$ can be expressed as:

$$H_{n_\varepsilon}(k) = H_0(k) \cdot e^{-j2\pi k n_\varepsilon / N} \quad k = 0 \ldots N-1 \tag{2.38}$$

where $H_0(k)$ is the CTF when no timing synchronization error occurs ($n_\varepsilon = 0$). The incremental rotation is the same for all symbols and does not pose a problem for demodulation. In the case of coherent modulation, the rotation can be easily compensated using reference pilots, whereas for differential modulation it is irrelevant since it does not change from symbol to symbol.

If n_ε is outside the allowed range, the amount of ISI depends on the symbol length N_U and on the actual channel power delay profile [85]. For the same n_ε, the effect depends on the symbol length. Larger symbols are less affected, as the relative overlap is lower. However, for a well designed system, the ISI levels are low and the error introduced can be treated as additional noise.

2.4.2. Carrier Frequency Offset

OFDM modulation is much more sensitive to frequency offsets than single-carrier modulation types, especially when the large symbols are used.

A frequency mismatch in the carrier frequency oscillator of the frontend mixer leads to a subcarrier frequency offset f_ε. The frequency error is directly translated to the baseband, so that for the same relative error, the absolute error in the baseband increases with the carrier frequency.

This frequency offset can be very large, but since it is constant it can be estimated and corrected during the receiver acquisition phase. In normal operation (tracking mode), only small residual offsets need to be considered.

The residual carrier frequency offset f_ε leads to an incremental rotation of the complex samples in time domain. In the following, the notation $f_{\varepsilon n}$ is used for the normalized frequency offset, i.e. relative to the sampling frequency f. The received signal affected by frequency offset becomes:

$$y_{rx}(n) = e^{j2\pi n f_{\varepsilon n}} y_{rx,ideal}(n) \tag{2.39}$$

Each sample, the complex signal suffers an incremental rotation of $2\pi\ f_{\varepsilon n}$. If the offset is correctly estimated, the compensation consists in rotating the signal with the same angle in the opposite direction.

The frequency offset is equivalent with a constant Doppler shift on all channel taps. Assuming correct symbol timing, the demodulated symbol s is given by the following equation [85]:

$$Y_{s,k} = \sum_{i=0}^{N-1} e^{j\pi\phi_{i,k}} e^{j2\pi((sN_S+N_G)/N)\phi_{i,k}} \frac{\sin(\pi\phi_{i,k})}{\pi\phi_{i,k}} X_{s,i} H_i \tag{2.40}$$

where H_i is the CTF at subcarrier i with no frequency offset, and $\phi_{i,k} = f_{\varepsilon n} N + i - k$.

The incremental rotation in time domain results in a shift of the subcarriers in frequency domain, as shown in **Figure 2.19**, thus leading to a loss of orthogonality. This phenomenon has two effects. On the one hand, the amplitude of each subcarrier is reduced, which affects the SNR. On the other hand, the subcarriers will leak into their neighbors, which causes ICI. The ICI components in (**2.40**) are obtained for $\forall i \neq k$.

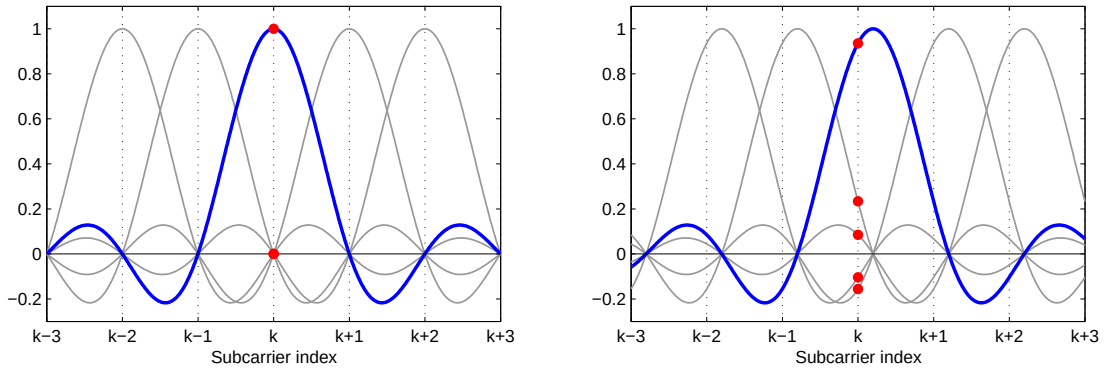

(a) $f_\varepsilon = 0$ (b) $f_\varepsilon = 0.2\Delta f$

Figure 2.19.: Effects of the frequency offset on the subcarrier orthogonality

The amount of ICI is proportional with the product $f_{\varepsilon n}N$ or $f_\varepsilon T_U$, which is the frequency shift relative to the subcarrier spacing $\Delta f = f/T_U$. If the frequency shift is small, the ICI components can be treated as additive noise $w_{s,k}$ and the *sinc* approximated with 1. Therefore, the expression of the demodulated symbol $Y_{s,k}$ becomes:

$$Y_{s,k} = e^{j\pi f_{\varepsilon n} N} e^{j2\pi(sN_S+N_G)f_{\varepsilon n}} X_{s,k} H_k + w_{s,k} \tag{2.41}$$

The time-invariant factor $e^{j\pi f_{\varepsilon n}N}$ cannot be distinguished from the complex subcarrier gain H_k and is treated as part thereof. The remaining complex phasor $e^{j2\pi(sN_S+N_G)f_{\varepsilon n}}$ indicates a rotation of all demodulated symbols $Y_{s,k}$ from one OFDM symbol to the next. The phase increment $\Delta\varphi$ is the same for all subcarriers:

$$\Delta\varphi = 2\pi(N + N_G)f_{\varepsilon n} \tag{2.42}$$

This rotation and thus the frequency offset is estimated using continuous pilots, inserted at certain subcarriers in all OFDM symbols. The estimate is used in a negative-feedback control loop, usually a PLL, which adjusts the compensating frequency so that the frequency offset and thus the incremental rotation become zero. With a careful design, the residual frequency shift can be minimized so that the SNR loss due to ICI becomes negligible.

The variance of the ICI noise σ_ε^2 can be approximated using the following relationship [11]:

$$\sigma_\varepsilon^2 \approx \frac{\pi^2}{3}\left(f_{\varepsilon n}N\right)^2 \tag{2.43}$$

2.4.3. Sampling Clock Frequency Offset

A frequency mismatch of the baseband sampling clock leads to a relative offset $\zeta = (T' - T)/T$, where T and T' are the sampling frequencies of the receiver and transmitter respectively.

This issue is especially of concern in consumer applications, where the crystal oscillators can have large tolerances, like 100 ppm. As with the carrier frequency offset, large mismatches can be corrected during the acquisition phase of the receiver, so that only small residual offsets remain in tracking mode.

The immediate effect of the sampling frequency offset is a resampling of the symbol, which leads to an accumulating timing error and thus a drift of the FFT window from the correct position. The exact sub-sample timing error for one symbol is ζN_S. A lower sampling frequency ($\zeta > 0$) leads to a positive timing error, i.e. the FFT window starts too late. The opposite is true for higher sampling frequencies.

For a DVB-T system in 8k mode, $N_S \approx 10^4$. Considering a crystal with a frequency tolerance of 100 ppm ($\zeta = \pm 10^{-4}$), the resulting timing error can be as high one sample per OFDM symbol.

A second effect of the sampling frequency offset is an incremental subcarrier symbol rotation. Unlike the case of the carrier frequency offset in (**2.42**), the phase increment between two consecutive OFDM symbols $\Delta\varphi$ depends now on the carrier index k. Subcarriers at the margins of the spectrum are affected the most. The new expression of $\Delta\varphi$ is [85]:

$$\Delta\varphi_k = 2\pi \frac{N_S}{N_U}(f_{\varepsilon n} N + \zeta k) \tag{2.44}$$

This relationship is depicted graphically in **Figure 2.20**. The dependence of the phase increment $\Delta\varphi$ on the subcarrier index k is a line with offset $2\pi\varphi_{\epsilon n} N_S$ and slope $2\pi\zeta N_S/N_U$. The offset depends linearly on the carrier frequency offset alone, while the slope depends linearly on the sampling frequency offset alone.

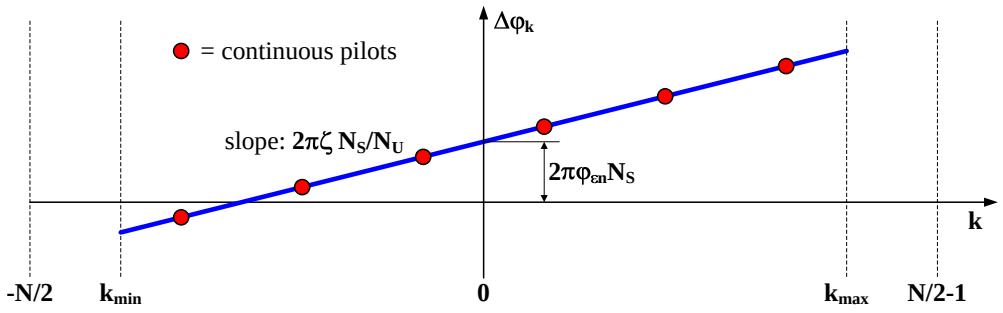

Figure 2.20.: Subcarrier symbol rotation in the presence of carrier and sampling clock offset

By using continuous pilots it is possible to estimate both the carrier and the sampling frequency

offset. The estimation is performed by determining the rotation angles of the pilots between two consecutive symbols, followed by a linear regression between these values.

The sampling frequency offset estimates are typically used in a delay-locked loop (DLL) to incrementally adjust the sampling instants with sub-sample resolution. This function can be implemented using a fractional rate converter (resampler) with a relatively wide phase accumulator to ensure an extremely fine sub-sample resolution. The phase accumulator increment is very close to unity. The small deviation from unity is adjusted by the DLL to that value which minimizes the sampling rate offset.

2.4.4. Additive Noise

The received signal is affected only by various impairments of the channel, as well as by imperfect synchronization in the receiver. The most important sources of signal errors are:

- Additive white Gaussian noise of the channel, W_n
- ICI due to channel Doppler fading, W_d
- ISI due to imperfect timing synchronization (symbol detection), W_t
- ICI due to imperfect frequency synchronization (carrier & sampling), W_f

If the interference levels (ICI & ISI) are low, their contribution can be approximated by an additive white noise. Considering the overall system noise, the demodulated FFT output $Y_{s,k}$ for symbol s and subcarrier k has the following expression:

$$Y_{s,k} = X_{s,k}H_{s,k} + W_{s,k} \tag{2.45}$$

where $X_{s,k}$ is the transmitted value and $H_{s,k}$ is the time-variant channel transfer function.

The noise term $W_{s,k}$ contains all four error sources mentioned before. Dropping the k and s indices, the expression of the overall noise contribution is:

$$W = W_n + W_d + W_t + W_f \tag{2.46}$$

It is important to realize that unlike W_t and W_f, which can be minimized by careful design, the Doppler W_d component is inevitable and cannot be minimized in the receiver. The synchronization units should be designed in such a way that the additional noise W_t and W_f is small compared to the thermal noise W_n. A rule of a thumb is that the remaining frequency offset f_ε must be less than 1% of the subcarrier spacing $\Delta f = 1/T_U$ and the timing error t_ε must be less than 0.1% of the useful symbol duration T_U [10]. Throughout this work, W_t and W_f are neglected compared to the thermal noise.

The real and the imaginary part of the noise are statistically independent (uncorrelated), with variance $\sigma_W^2 = 1/SNR_W$, where the average power of the data cells is one. Both σ_W^2 and SNR_W refer to the frequency domain. We also denote with σ_w^2 and SNR_w the same quantities in time domain before guard interval removal, which are a property of the channel. The relationship between the two SNR's can be determined by knowing that the symbol energy decreases after guard interval removal, whereas the noise variance remains the same. The guard interval causes therefore an effective SNR degradation that can be expressed as:

$$\frac{SNR_W}{SNR_w} = \frac{N_U}{N_S} = \frac{N_S - N_G}{N_S} \tag{2.47}$$

The SNR degradation can also be expressed in dB as $10\log_{10}(1 - N_G/N_S)$. For a given channel SNR, the noise variance in frequency domain increases linearly with the length of the guard interval N_G. These considerations are true only when the guard interval is a cyclic prefix.